Geophysical Research Letters

RESEARCH LETTER
10.1029/2024GL111131

Special Collection:
Slow to fast earthquakes and the geology, structure, and rheology of their host subduction zones

Prediction of Complex Observed Shear Wave Splitting Patterns at Ryukyu Subduction Zone Using a Strong Intra-Slab Anisotropy Model

Sharmila Appini[1], Jiaxuan Li[1], Hao Hu[1,2], Neala Creasy[3], Leon Thomsen[1], Joseph McNease[1], and Yingcai Zheng[1]

[1]Department of Earth and Atmospheric Sciences, University of Houston, Houston, TX, USA, [2]School of Geosciences, The University of Oklahoma, Norman, OK, USA, [3]Los Alamos National Laboratory, Los Alamos, NM, USA

Abstract Complex shear wave splitting (SWS) patterns in subduction zones are often interpreted geodynamically as resulting from complex mantle flow; however, this may not always be necessary. We analyzed 7,093 high-quality SWS measurements from teleseismic S waves recorded by Hi-net stations across the Ryukyu arc in Japan. Our findings show a systematic rotation of the fast S polarization from trench-parallel to trench-perpendicular depending on the earthquake backazimuth. For the same earthquake, the measured splitting patterns also vary spatially across the southwest Japan. Using full-wave seismic modeling, we showed that a dipping slab with ∼30% shear anisotropy of the tilted transverse isotropy (TTI) type, with a symmetry axis perpendicular to the slab interface, can predict the observed delay times and polarization rotation. Our results highlight the importance of considering dipping anisotropic slabs in interpreting SWS at subduction zones.

Plain Language Summary Seismic anisotropy is used to characterize rock fabric, which encodes important information about its stress and deformation history. In an anisotropic rock, seismic waves travel at different speeds along different propagation directions. Furthermore, a shear wave can split into a fast and a slow shear wave after passing through an anisotropic medium, known as shear wave splitting (SWS). While many studies have attributed the observed anisotropy primarily to large-scale mantle flows around the subducting slab, the role of the subducting slab itself has often been overlooked. Recent research shows shear anisotropy inside slabs to be ∼30% and it is of great scientific value to test if this model can produce the observed complex SWS. To test this hypothesis, we measured SWS patterns recorded by Hi-net stations in southwest Japan, where shear waves passed through the Ryukyu slab. We found that a dipping anisotropic slab model can explain the observations very well. This work demonstrates that complex SWS patterns could be caused by strong slab anisotropy, not necessarily mantle flows, impacting how we understand mantle dynamics.

Key Points:

- We made 7,093 shear wave splitting measurements for teleseismic S waves recorded by Hi-net stations in Japan
- We observed that shear wave splitting pattern changes systematically with earthquake backazimuth
- We can explain this with a dipping slab having ∼30% intra-slab shear anisotropy, derived from previous analyses of non-double-couple earthquake moment tensors

Supporting Information:

Supporting Information may be found in the online version of this article.

Correspondence to:

S. Appini,
sappini@uh.edu

Citation:

Appini, S., Li, J., Hu, H., Creasy, N., Thomsen, L., McNease, J., & Zheng, Y. (2025). Prediction of complex observed shear wave splitting patterns at Ryukyu subduction zone using a strong intra-slab anisotropy model. *Geophysical Research Letters*, *52*, e2024GL111131. https://doi.org/10.1029/2024GL111131

Received 11 AUG 2024
Accepted 20 JAN 2025

Author Contributions:

Conceptualization: Yingcai Zheng
Data curation: Sharmila Appini
Formal analysis: Sharmila Appini, Neala Creasy, Joseph McNease, Yingcai Zheng
Funding acquisition: Yingcai Zheng
Investigation: Sharmila Appini, Jiaxuan Li, Hao Hu, Neala Creasy, Leon Thomsen, Joseph McNease, Yingcai Zheng
Methodology: Yingcai Zheng

1. Introduction

Shear-wave splitting (SWS) studies in subduction zones often tend to ignore anisotropy in seismic velocity within the subducting slab, because of the relatively short seismic raypath in the slab and perceived weak seismic anisotropy within slabs. Such a practice could be justified only if the intra-slab shear anisotropy is weak. However, analyses of deep earthquake moment tensors (Li et al., 2018; Vavrycuk, 2004, 2006) suggested the slab to be highly anisotropic. It compels us to ask the following questions: how does a strongly anisotropic dipping slab (or part of it) affect the SWS patterns at subduction zones? To what degree can such a medium explain the observed complex SWS pattern?

Because the seismic moment tensor can be mathematically related to the full elastic anisotropy tensor in the dislocation source region (Aki & Richards, 2002), it provides a basis for direct anisotropy parameter inversion using moment tensors, especially using the non-double-couple-components (ndcc). Strong intra-slab anisotropy has been found in multiple studies. For example, earlier regional works by Vavrycuk (2004, 2006) obtained high anisotropic values (∼10%) in Tonga for both P and S waves by assuming an orthorhombic anisotropy of a mineralogical origin. More recently, Li et al. (2018) did a comprehensive global study and analyzed moment tensors (Ekström et al., 2012) of deep earthquakes in six subduction systems. They found that a highly anisotropic fabric of the tilted transverse isotropy (TTI) type, with a symmetry axis mostly perpendicular to the slab interfaces, and up to >40% shear anisotropy (with a typical value around ∼25%–30%), could explain the observed ndcc in those slabs. Such a strong anisotropy is unlikely to originate from the intrinsic elastic properties of

Project administration: Yingcai Zheng
Resources: Yingcai Zheng
Software: Sharmila Appini, Hao Hu, Yingcai Zheng
Supervision: Yingcai Zheng
Validation: Sharmila Appini, Jiaxuan Li, Joseph McNease, Yingcai Zheng
Visualization: Sharmila Appini
Writing – original draft: Sharmila Appini
Writing – review & editing: Sharmila Appini, Jiaxuan Li, Hao Hu, Neala Creasy, Leon Thomsen, Yingcai Zheng

common mantle-forming minerals such as olivine and pyroxene (Jung & Karato, 2001; Karato et al., 2008; Mainprice & Ildefonse, 2009; Wang et al., 2017). Li et al. (2018) attributed the origin of such a fabric to sheet silicates, water/melt pockets, carbonates/magnesites due to metamorphic reactions, and their shearing deformation in slabs. Other high-resolution seismic analyses using favorable ray geometry also obtained strong intra-slab anisotropy (e.g., Eakin et al., 2016; Nowacki et al., 2015; Song & Kim, 2012). Audet (2013) used receiver function analysis and showed that the top of the subducted slab can be 10%–25% anisotropic.

When a shear wave travels through an anisotropic medium, it could split into two polarized shear waves propagating at different speeds. By measuring the delay time between the fast and slow S waves and their polarizations recorded by the same seismic station, we can infer the overall anisotropy along the ray path (e.g., Crampin & Peacock, 2008; Lynner & Long, 2015; Nakajima & Hasegawa, 2004; Silver & Chan, 1991; Song & Kawakatsu, 2012). When there is substantial anisotropy within the intra-slab region such as those values, ∼25% obtained by Li et al. (2018), the predicted splitting times can be significant (>1 s), despite the short teleseismic raypath traveled inside the slab.

A dipping anisotropic layer can also cause different SWS patterns depending on earthquake locations. Song and Kawakatsu (2012) studied the SWS delay times in statistics due to a dipping sub-slab anisotropic layer in multiple subduction zones. It is also found that the fast S polarization can be either trench-parallel, or trench-perpendicular, or at an intermediate angle. In observation, various studies have shown the existence of anisotropy in subduction zones, especially in Japan. Many of them used SWS analysis to illustrate the anisotropy present in the upper crust (e.g., Kaneshima et al., 1988; Saiga et al., 2003), mantle wedge (e.g., Long & van der Hilst, 2006; Salah et al., 2009), or upper mantle region (e.g., Iidaka et al., 2009; Long & van der Hilst, 2005), and sub-slab region (e.g., Song & Kawakatsu, 2012). In these studies, both trench-parallel and trench-perpendicular fast directions have been observed (e.g., Long & van der Hilst, 2005; Nakajima & Hasegawa, 2004; Wirth & Long, 2010). A few of these studies also found significant lateral variation in the fast S polarization across the Japan region, interpreted as distinct forms of anisotropy, arising from factors such as the deformation of B-type olivine fabric from preferred orientation of minerals due to mantle flow (e.g., Kneller et al., 2005; Kneller et al., 2007; Kneller et al., 2008; Lassak et al., 2006; Long et al., 2007). Additionally, the effects of complicated anisotropic models on SWS measurements have also been explored. Some have considered multi-layered anisotropy (Levin et al., 1999; Ozalaybey & Savage, 1994; Silver & Savage, 1994), dipping symmetry axes (Chevrot, 2000; Chevrot & Van Der Hilst, 2003; Hartog & Schwartz, 2000), and variation in fast S polarization direction with depth (Saltzer et al., 2000).

Here, we adopt a similar procedure by Song and Kawakatsu (2012) to evaluate the slab anisotropy model from Li et al. (2018). Instead of performing a statistical comparison, we will make quantitative SWS predictions for each station using a dipping anisotropic subducting slab represented as a TTI medium, with symmetry axis perpendicular to the slab interface. By "anisotropic slab", we do not imply that the entire slab is anisotropic but rather a part of it. Although Li et al. (2018) can directly give the anisotropy strength and TTI symmetry axis, their results cannot determine the thickness of the anisotropy region. However, the thickness is estimated to be >∼ 20 km (Li et al., 2018), based on the dimensions of the earthquake sources. In our modeling, the thickness of the dipping anisotropic layer will be a free parameter. We consider earthquake backazimuth and seismic ray incident angle, as well as slab anisotropy in our SWS predictions.

It is not our intention to perform an anisotropy inversion or tomography along the teleseismic S ray path. Instead, we use the anisotropy model of intra-slab TTI anisotropy that has been already obtained (Li et al., 2018) and the Slab 2.0 geometry (Hayes et al., 2018) to make quantitative SWS predictions for each station and compare them with the observations. We focus solely on evaluating the hypothesis that how well a dipping anisotropic structure in the slab explains the observed SWS, without considering possible anisotropy sources elsewhere. Although we used ∼3,430 observed SWS data points of diverse source-receiver azimuths and ray incident angles, we only adjust one free parameter, which is the thickness of the anisotropic layer, to fit the data.

2. Data and Methods

For this study, we utilized the 3-component seismic data recorded by the Japan Hi-net seismic network (Figure 1), which has about 800 stations. We selected the southwest Japan region as our study area due to the abundant availability of high-quality direct S arrivals. To evaluate our hypothesis, we covered a wide backazimuthal range of 120°–240° around Japan by considering teleseismic events between March 2004–January 2020 with focal

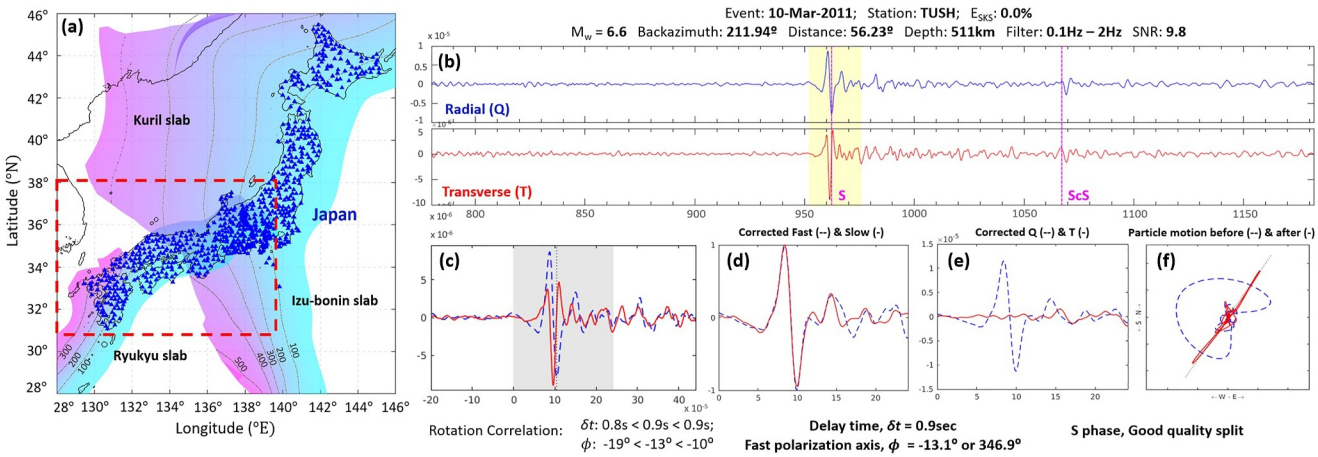

Figure 1. (a) Map showing the entire 795 Hi-net stations (blue triangles) in Japan along with slab interfaces from the Slab 2.0 model (Hayes et al., 2018). The black dashed lines labeled by numbers (e.g., 100, 200, etc. with unit in km) are the slab depth contours. The red box indicates our study region in SW Japan region above the Ryukyu slab of the Philippine Sea Plate. (b) QT—radial (Q or SV) and transverse (T or SH) components. The highlighted (yellow) region marks the data window for splitting measurement: (c) raw Q (blue dashed) and T (red solid) waveforms before anisotropy correction; (d) fast (blue dashed) and slow (red solid) components after anisotropy correction; (e) Q (blue dashed) and T (red solid) components after the correction; (f) elliptical particle motion before (blue dashed) and linearized (red solid) after correction.

depths greater than 60 km and Mw > 5.5. It results in 660 selected deep earthquakes. Most of our high-quality direct S splitting measurements are from the deep earthquakes in the Tonga and Java regions, with epicentral distances greater than 60° and backazimuths varying from 120° to 150°. We also collected and analyzed teleseismic ScS, SKS and SKKS phases. However, we got much fewer SWS measurements for SKS and SKKS phases. It may be because the Hi-net stations are short-period seismometers and the SKS waves are commonly examined in the frequency range of 0.02–0.5 Hz (e.g., Karlowska et al., 2021; Long & van der Hilst, 2005). For these reasons, we only used the direct S phases in this study. We measured SWS parameters of teleseismic S phases (Figure S1 in Supporting Information S1) for epicentral distances beyond 40°, with ray incident angles at the stations up to 28°, from the vertical direction. The limited ScS phase records are also shown in Figure S2 of Supporting Information S1.

We use the SplitLab software (Wüstefeld et al., 2008) to measure SWS parameters. Due to the excellent backazimuth coverage, this data set offers the opportunity for us to characterize the backazimuth dependence of SWS in detail. The splitting parameters—delay time (δt) and fast-S polarization direction (ϕ) of each source-receiver pair are estimated using the rotation-correlation method (Bowman & Ando, 1987; Fukao, 1984), after applying a Butterworth filter of 0.1–2 Hz to the waveforms.

We adopt the following criteria for quality control in our SWS measurement: (a) the maximum correlation coefficient is greater than 0.8; (b) the particle motion exhibits linearity after rotation; (c) results should also be consistent with those from the eigenvalue method (Savage, 1999; Silver & Chan, 1991), since this approach does not assume that the initial wave polarization is known. However, the errors reported in the data sets (presented in Data set S1 and Data set S2) are likely smaller than should be the case, as discussed by Walsh et al. (2013). We assign: "good", "fair", or "poor", to the SWS measurement based on factors such as waveform quality, particle motion, and consistency among different splitting measurement methods (using visual inspection). To demonstrate our SWS measurement procedure, we show a seismic record of a deep earthquake (depth at 511 km) at station TUSH in Figures 1b–1f along with a step-by-step description in Text S1 of Supporting Information S1.

3. Results

3.1. Observation—Splitting Measurement Results

Through visual inspection of over 135,000 records of teleseismic S, ScS, SKS and SKKS phases at Hi-net stations, we made 7,081 splitting measurements of adequate quality ("good" and "fair") covering the entire Japan. See our data availability statement. Among these, a substantial proportion of reliable results (~3,430 records) belong to direct S phases in the SW Japan region. Our final SWS results consist of both event and station

10.1029/2024GL111131

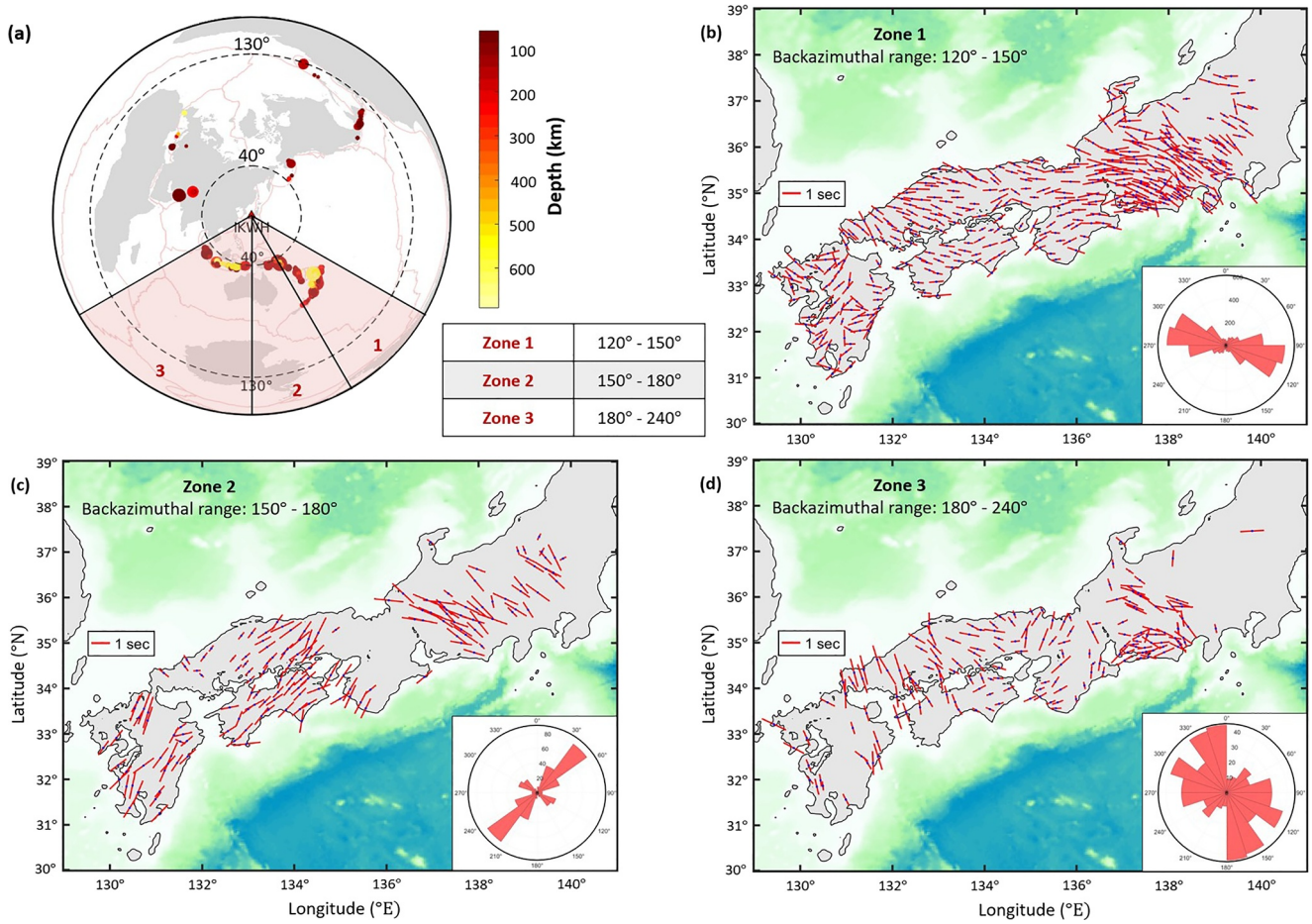

Figure 2. Measured and averaged shear wave splitting results. (a) Three earthquake backazimuthal zones. (b–d) Averaged teleseismic S-phase splitting patterns for earthquakes in Zone 1, Zone 2, and Zone 3, respectively. Inset rose diagrams show fast-S polarizations of all the stations. The radius corresponds to the number of measurements in that angular sector.

information, event backazimuth, angle of incidence at the station, splitting time, fast-S polarization, and quality rating of the measurements. Null observations are also included in the results, characterized by a linear or near-linear initial particle motion and small delay times, close to zero.

Given that our objective is to evaluate the SWS patterns due to a dipping TTI slab, we deliberately choose specific backazimuthal ranges where the seismic raypaths can intersect the slab, shown in Figure 2a. Based on the event distribution and backazimuth, we group the events into three backazimuthal zones/sectors. Zone 1 mainly consists of distant events with greater focal depths in Tonga and a mixture of events with varying epicentral distances. Zone 2 and Zone 3 feature the events that are much closer in proximity to the southwest Japan, especially in Java.

For each seismic station, we measured the delay times and fast S polarization directions for all the earthquakes in each zone. We then averaged over the earthquakes the measured SWS patterns (both delay time and the fast S polarization) for each station. These averaged measurements of SWS parameters in every backazimuthal zone are shown in Figures 2b–2d.

The splitting measurements reveal two key observations: (a) a striking consistency in SWS patterns among earthquakes within each backazimuthal zone at most stations (see Figure S1 in Supporting Information S1), justifying the averaging of SWS parameters in Figure 2; and (b) notable spatial variations in fast-S polarization directions from west to east, corresponding to the orientation changes in the Philippine Sea Slab, particularly in Zones 2 and 3 (Figures 2c and 2d). Moreover, at the same station, fast-S polarization directions vary for events in different zones. For instance, stations located west of 132°E exhibit trench-parallel orientations in Zone 2, but

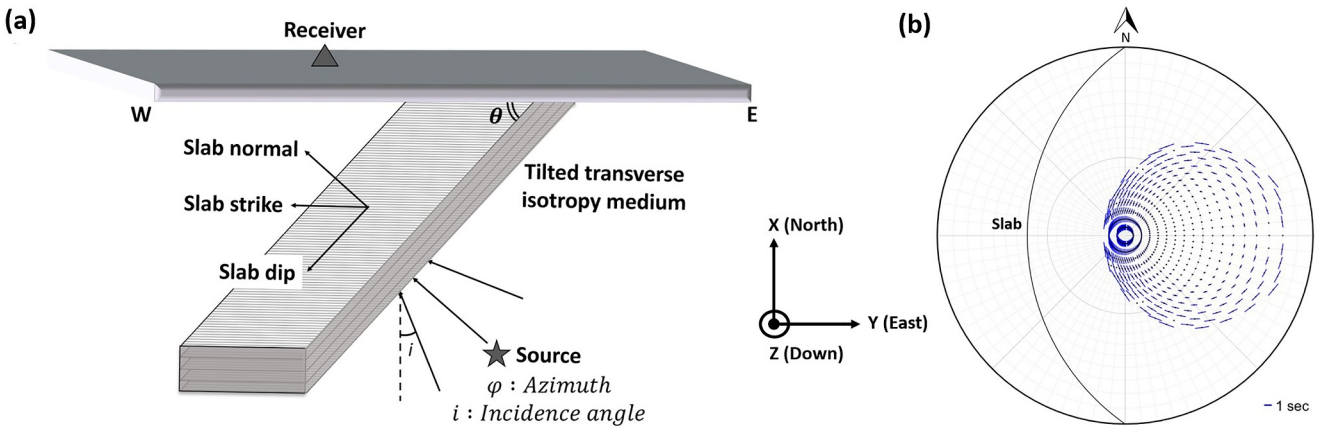

Figure 3. 3D modeling of SWS for plane S wave propagation through a dipping anisotropic layer. (a) A schematic showing the dipping anisotropic layer and plane wave incident geometry. The slab is dipping toward the west at an angle, $\theta = 35°$. The anisotropic layer is 20 km thick and has a tilted transverse isotropy (TTI) type anisotropy: the P-wave anisotropy is zero, the S-wave anisotropy is 0.3 and the Thomsen's δ is zero. The conversion of Thomsen parameters to elastic tensors is outlined in Thomsen (1986). Propagating along the TTI symmetry axis in the anisotropic layer, the P-wave velocity, V_P is 8.4 km/s, and the S-wave velocity, V_S is 4.67 km/s. The upper and lower layers are isotropic half-spaces and have the same $V_P = 8$ km/s and $V_S = 4.45$ km/s. The rock density is set to be uniform (3400 kg/m^3) in the whole model. The angle φ (measured clockwise from the north) is the azimuth of the incident raypath and angle i is the incident angle with respect to the vertical direction. (b) Lower hemisphere stereographic projection used to show the dipping slab (labeled "Slab"). The blue bar location (or its midpoint) shows the incident SV plane wave backazimuth and incident angle in the same projection. The orientations of the blue bars show the fast-S polarization vector, and their lengths are proportional to the delay time, with a 1.0 s scale shown at the lower right location.

trench-perpendicular in Zone 3. These observations imply that the near-receiver structure, or possibly the slab configuration and strong anisotropy within the slab, may be the cause of such a spatial variation.

3.2. Prediction—Modeling SWS Parameters for a Dipping Anisotropic Slab

We predicted splitting parameters for shear waves as they traverse a dipping slab of the TTI type anisotropy, using full-waveform forward modeling. There have been many theoretical and numerical advancements in wave propagation within a dipping anisotropic layer, based on ray theory or full-wave modeling (e.g., Chevrot & Van Der Hilst, 2003; Frederiksen & Bostock, 2000; Maupin & Park, 2007; Romanowicz & Yuan, 2012; Song & Kawakatsu, 2012). Our approach employs a 3D full-wave modeling with the propagator matrix method (Haskell, 1953; Mallick & Frazer, 1991). We could incorporate arbitrary anisotropy in our propagator matrix method and use plane wave incidence. This technique enabled us to compute and predict SWS patterns that would be observed at Earth's surface stations for a dipping layered medium (Figure 3a). We have benchmarked our modeling code against a finite difference code (Fang et al., 2017) and they produced identical waveforms. We generated 3-component synthetic seismograms for different plane wave incident angles in a three-layered medium, where the middle layer is tilted representing the anisotropic part of the slab. We then used the same measurement technique discussed previously to measure the delay time and fast-S polarization using the modeled waveforms.

Our modeled results show that SWS parameters are indeed dependent upon the incoming wave azimuth and the incidence angle (Figure 3b). The fast-S polarization can manifest as either trench-parallel or trench-perpendicular, and the splitting time can exceed 1.0 s. While this feature has previously been reported by Song and Kawakatsu (2012) in the context of investigating sub-slab anisotropy, our objective centers on exploring intra-slab anisotropy of the TTI type symmetry. Song and Kawakatsu (2012) put anisotropy of the orthorhombic type in sub-slab region to explain SKS splitting. However, the moment-tensor derived strong anisotropy by Li et al. (2018) cannot be explained by the preferred orientation of olivine (max∼22%) (Mainprice et al., 2007) in mantle flows, in supra-slab or sub-slab regions. The maximum anisotropy strength for natural olivine ranges within 5%–15% and the B-type olivine through which both teleseismic and local-S rays travel, exhibits anisotropy up to 12% (Kneller et al., 2008).

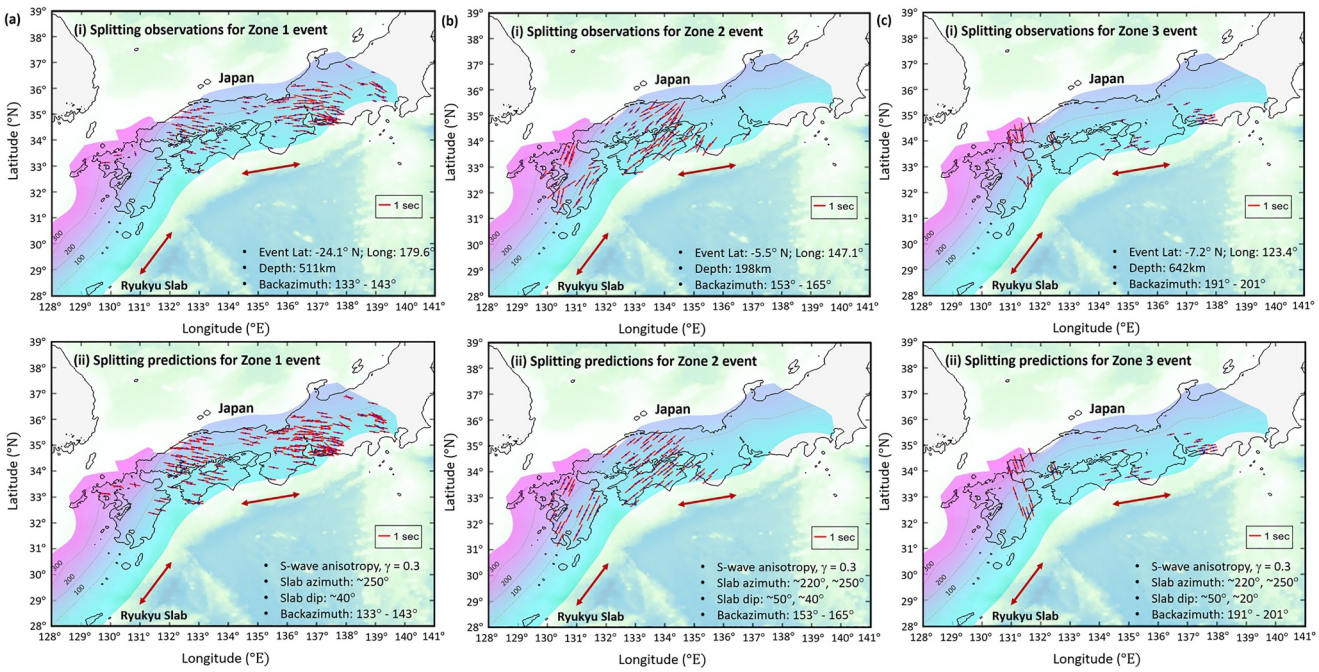

Figure 4. Comparison between predicted and observed SWS patterns (a–c). (i) SWS observations from a single event located in each zone (Zones 1, 2 and 3). The event information is presented at the lower right location in panels labeled as (i). The thick red double-arrows represent the slab strike directions. (ii) Corresponding SWS predictions using the same event. Here, the modeling parameters are as follows: P-wave anisotropy $\varepsilon = 0.1$, S-wave anisotropy $\gamma = 0.3$ and the Thomsen's $\delta = 0.1$.

3.3. Comparison Between Predictions and Observations

Using the earthquake moment tensors from the Global Centroid Moment Tensors catalog (Dziewonski et al., 1981; Ekström et al., 2012), Li et al. (2018) determined the intra-slab anisotropy of 6 different subducting slabs. In the case of Japan slab, the shear anisotropy strength γ exhibits a range between 6% and 38%. Hence, we develop a slab model characterized by shear wave anisotropy, $\gamma = 0.3$, equivalent to ∼30%. We set our free parameter, the thickness of the anisotropic portion of the slab, to be 40 km. Considering the changes in orientation from west to east in the Ryukyu slab, we incorporate the slab geometry from the Ryukyu slab 2.0 model (Hayes et al., 2018). Consequently, we employ a 1-D ray tracing technique built in the CrazySeismic package (Yu et al., 2017) to determine the piercing point of the incident S-wave at the slab interface to establish local incident/transmission angles. We also determine the slab local strike and dip at each piercing point, and compute waveforms with the propagator matrix approach described earlier. Finally, the same rotation correlation method in SplitLab, is applied to measure the SWS parameters, both the delay time and the polarization.

The Ryukyu slab has different strike angles from west to east (Figure 4). In the western section, the average slab strike is ∼220° and for the eastern section it is ∼250°. Because we have observed consistent SWS patterns among different earthquakes in each earthquake zone (Figure S1 in Supporting Information S1), we pick one representative earthquake from each zone and show the predicted and observed SWS patterns (Figure 4). Our results show a remarkable similarity between SWS observations (in both fast-S polarizations and delay times) measured from real earthquake data and our predicted results using a dipping anisotropic slab model.

4. Discussion

Our hypothesis is that a strong TTI slab (or part of it) can cause the observed event-backazimuth dependent SWS patterns. In testing this hypothesis, we did not consider the existence of possible anisotropy in other regions. However, this work is a feasibility study rather than an inversion anisotropy everywhere in the subduction zone. If the answer to our hypothesis is negative, we need to abandon this idea and then focus our efforts on mapping anisotropy in areas other than the slab. Nevertheless, our results show that a ∼40 km thick, dipping TTI medium in the slab, can explain the observed complex and variable SWS patterns for earthquakes from different back-azimuths, despite having only one free parameter in our modeling (i.e., the thickness of the TTI anisotropic layer).

Both the simplicity of the hypothesis and its prediction power lend credibility to the merit of our hypothesis. The dipping TTI medium considered here could be from aligned melt pockets (e.g., Shirey et al., 2021; Thomsen, 1995), or hydrous minerals like serpentines, which can exhibit up to 32% shear-wave anisotropy, much stronger than olivine anisotropy (Katayama et al., 2009). Methods like high-resolution seismic attenuation (Abers et al., 2006) can detect the presence of fluids or hydrous phases in the slab. For the overriding plate, neither VTI nor HTI could produce the observed backazimuth-dependent SWS patterns. A thicker TTI layer with weaker anisotropy outside the slab region might also produce similar SWS patterns, but determining the thickness and anisotropy distribution requires further investigation.

On the other hand, the effect of the source side anisotropy needs to be also considered because the splitting of a telesesimic S phase can be influenced by anisotropy within the source region. Here, we use "source-side anisotropy" to denote the anisotropic effect on the incident wave common to all the Hi-net stations. This anisotropy is typically estimated by analyzing the splitting of direct S waves, incorporating receiver side-corrections inferred from SKS wave analyses (Nowacki et al., 2015; Song & Kawakatsu, 2012). In this paper, we propose a new approach. We assume that potential anisotropy around the teleseismic earthquakes and along the path has already split the incident S waves, into a fast S and a slow S, upon incidence on the Ryukyu slab. We can use three parameters to characterize such a scenario: the polarization angle of the incident fast S (the slow S polarization is perpendicular to the fast S), the delay time (dt_{inc}) between the fast and slow S, and the amplitude ratio between the two S waves. Together with the thickness of the anisotropic layer in the slab, the degrees of freedom are four, still a very small number compared to the large number of constraints (e.g., thousands of SWS measurements). We perform grid search of the three parameters, conduct full-waveform modeling, and measure SWS of the recorded waves to assess their impact on SWS. The procedure is detailed as follows. We start by using the earthquake moment tensor from the Global Centroid Moment Tensor (GCMT) catalog to compute the SV and SH components of the particle motion, following Aki and Richards (2002). SV-SH in the isotropic Earth forms a coordinate plane perpendicular to the ray path (Figure S3a in Supporting Information S1). We then vary the incident fast S polarization angle by an angle θ with respect to the SV direction. The slow S polarization will be orthogonal ($90° + \theta$) with respect to the SV component. A time delay, dt_{inc}, is then introduced to the incident slow S wave (Figure S3b in Supporting Information S1). Initially, we set $\theta = 0°$ with no time delay between the incident SV and SH waves and test the incidence of different SV and SH amplitude ratios (Figure S4; Text S2 in Supporting Information S1) for their impacts on SWS. We then extend the analysis to $\theta = 30°$, 45° and 60°, introduce a time delay, $dt_{inc} = 1.0$ s, between the fast and the slow S, model the waveforms, and measure the SWS parameters (Figures S5–1 ~ 3; Text S2 in Supporting Information S1). Across all these cases (Figures S4 and S5 in Supporting Information S1), the splitting results remain minimally affected, as they hardly alter the waveform shape in the two horizontal components. Thus, the effect of source-side anisotropy on splitting is not as strong compared to the intra-slab anisotropy effect based on our tests.

5. Conclusions

Recent work has established that a strong TTI anisotropy in slab can produce the observed ndcc in moment tensors. Can such anisotropy also predict the observed SWS patterns, especially their dependence on the earthquake backazimuth? To investigate this, we curated and processed an extensive database, comprising SWS measurements of teleseismic S phases recorded by the Hi-net array in SW Japan. For events with backazimuths ranging from 120° to 240°, the measured SWS parameters are complex and dependent on earthquake backazimuths. The spatial variations observed in these parameters across SW Japan, for the same earthquake, emphasize the significant role of intra-slab anisotropy. If we place all possible anisotropy in the dipping slab, we can predict the complex SWS patterns by a dipping intra-slab TTI region with a thickness of ~40 km and ~30% shear anisotropy, and the predictions agree with the observations. Our work demonstrates that complex SWS observed at subduction zones can be explained without invoking complex mantle flow geodynamic models.

Data Availability Statement

The 3-component seismogram data utilized in this study is freely accessible through NIED Hi-net, managed by the National Research Institute for Earth Science and Disaster Resilience (NIED, 2019). The SplitLab software package, based on MATLAB, is available from Wüstefeld et al. (2008). We also provide our SWS processed

results (including those shown in Figure S1 of Supporting Information S1) as a data set in Excel file deposited in the Texas Data Repository (Appini et al., 2025).

Acknowledgments
We thank Dr. Romanowicz and an anonymous reviewer for their constructive comments which helped improve our manuscript. We also appreciate Dr. Germán Prieto, the editor, and Dr. Ake Fagereng, the associate editor, for their valuable feedback and guidance throughout the review process. This work is funded by NSF EAR-2027150.

References

Abers, G. A., van Keken, P. E., Kneller, E. A., Ferris, A., & Stachnik, J. C. (2006). The thermal structure of subduction zones constrained by seismic imaging: Implications for slab dehydration and wedge flow. *Earth and Planetary Science Letters*, *241*(3–4), 387–397. https://doi.org/10.1016/j.epsl.2005.11.055

Aki, K., & Richards, P. G. (2002). *Quantitative seismology*. University Sciences Books.

Appini, S., Li, J., Hu, H., Creasy, N., Thomsen, L., McNease, J., & Zheng, Y. (2025). Dataset: Teleseismic shear wave splitting measurements from Hi-net stations in Japan [Dataset]. *Texas Data Repository*. https://doi.org/10.18738/T8/SDDR6Q

Audet, P. (2013). Seismic anisotropy of subducting oceanic uppermost mantle from fossil spreading. *Geophysical Research Letters*, *40*(1), 173–177. https://doi.org/10.1029/2012gl054328

Bowman, J. R., & Ando, M. (1987). Shear-wave splitting in the upper-mantle wedge above the Tonga subduction zone. *Geophysical Journal International*, *88*(1), 25–41. https://doi.org/10.1111/j.1365-246x.1987.tb01367.x

Chevrot, S. (2000). Multichannel analysis of shear wave splitting. *Journal of Geophysical Research*, *105*(B9), 21579–21590. https://doi.org/10.1029/2000jb900199

Chevrot, S., & Van Der Hilst, R. D. (2003). On the effects of a dipping axis of symmetry on shear wave splitting measurements in a transversely isotropic medium. *Geophysical Journal International*, *152*(2), 497–505. https://doi.org/10.1046/j.1365-246x.2003.01865.x

Crampin, S., & Peacock, S. (2008). A review of the current understanding of seismic shear-wave splitting in the earth's crust and common fallacies in interpretation. *Wave Motion*, *45*(6), 675–722. https://doi.org/10.1016/j.wavemoti.2008.01.003

Dziewonski, A. M., Chou, T. A., & Woodhouse, J. H. (1981). Determination of earthquake source parameters from waveform data for studies of global and regional seismicity. *Journal of Geophysical Research*, *86*(Nb4), 2825–2852. https://doi.org/10.1029/jb086ib04p02825

Eakin, C. M., Long, M. D., Scire, A., Beck, S. L., Wagner, L. S., Zandt, G., & Tavera, H. (2016). Internal deformation of the subducted Nazca slab inferred from seismic anisotropy. *Nature Geoscience*, *9*(1), 56–59. https://doi.org/10.1038/ngeo2592

Ekström, G., Nettles, M., & Dziewonski, A. M. (2012). The global cmt project 2004–2010: Centroid-moment tensors for 13,017 earthquakes. *Physics of the Earth and Planetary Interiors*, *200*, 1–9. https://doi.org/10.1016/j.pepi.2012.04.002

Fang, X. D., Zheng, Y. C., & Fehler, M. C. (2017). Fracture clustering effect on amplitude variation with offset and azimuth analyses. *Geophysics*, *82*(1), N13–N25. https://doi.org/10.1190/geo2016-0045.1

Frederiksen, A. W., & Bostock, M. G. (2000). Modelling teleseismic waves in dipping anisotropic structures. *Geophysical Journal International*, *141*(2), 401–412. https://doi.org/10.1046/j.1365-246x.2000.00090.x

Fukao, Y. (1984). Evidence from core-reflected shear-waves for anisotropy in the Earths mantle. *Nature*, *309*(5970), 695–698. https://doi.org/10.1038/309695a0

Hartog, R., & Schwartz, S. Y. (2000). Subduction-induced strain in the upper mantle east of the Mendocino triple junction, California. *Journal of Geophysical Research*, *105*(B4), 7909–7930. https://doi.org/10.1029/1999jb900422

Haskell, N. A. (1953). The dispersion of surface waves on multilayered media. *Bulletin of the Seismological Society of America*, *43*(1), 17–34. https://doi.org/10.1785/bssa0430010017

Hayes, G. P., Moore, G. L., Portner, D. E., Hearne, M., Flamme, H., Furtney, M., & Smoczyk, G. M. (2018). Slab2, a comprehensive subduction zone geometry model. *Science*, *362*(6410), 58–61. https://doi.org/10.1126/science.aat4723

Iidaka, T., & Hiramatsu, Y., & O. Japanese Univ Grp Joint Seismic. (2009). Shear-wave splitting analysis of the upper mantle at the Niigata-Kobe tectonic zone with the data of the joint seismic observations at Nktz. *Earth Planets and Space*, *61*(2), 227–235. https://doi.org/10.1186/bf03352903

Jung, H., & Karato, S. (2001). Water-induced fabric transitions in olivine. *Science*, *293*(5534), 1460–1463. https://doi.org/10.1126/science.1062235

Kaneshima, S., Ando, M., & Kimura, S. (1988). Evidence from shear-wave splitting for the restriction of seismic anisotropy to the upper crust. *Nature*, *335*(6191), 627–629. https://doi.org/10.1038/335627a0

Karato, S., Jung, H., Katayama, I., & Skemer, P. (2008). Geodynamic significance of seismic anisotropy of the upper mantle: New insights from laboratory studies. *Annual Review of Earth and Planetary Sciences*, *36*(1), 59–95. https://doi.org/10.1146/annurev.earth.36.031207.124120

Karlowska, E., Bastow, I. D., Rondenay, S., Martin-Short, R., & Allen, R. M. (2021). The development of seismic anisotropy below South-central Alaska: Evidence from local earthquake shear wave splitting. *Geophysical Journal International*, *225*(1), 548–554. https://doi.org/10.1093/gji/ggaa603

Katayama, I., Hirauchi, H., Michibayashi, K., & Ando, J. (2009). Trench-parallel anisotropy produced by serpentine deformation in the hydrated mantle wedge. *Nature*, *461*(7267), 1114–U1209. https://doi.org/10.1038/nature08513

Kneller, E. A., Long, M. D., & van Keken, P. E. (2008). Olivine fabric transitions and shear wave anisotropy in the Ryukyu subduction system. *Earth and Planetary Science Letters*, *268*(3–4), 268–282. https://doi.org/10.1016/j.epsl.2008.01.004

Kneller, E. A., van Keken, P. E., Karato, S., & Park, J. (2005). B-type olivine fabric in the mantle wedge: Insights from high-resolution non-Newtonian subduction zone models. *Earth and Planetary Science Letters*, *237*(3–4), 781–797. https://doi.org/10.1016/j.epsl.2005.06.049

Kneller, E. A., van Keken, P. E., Katayama, I., & Karato, S. (2007). Stress, strain, and b-type olivine fabric in the fore-arc mantle: Sensitivity tests using high-resolution steady-state subduction zone models. *Journal of Geophysical Research*, *112*(B4). https://doi.org/10.1029/2006jb004544

Lassak, T. M., Fouch, M. J., Hall, C. E., & Kaminski, E. (2006). Seismic characterization of mantle flow in subduction systems: Can we resolve a hydrated mantle wedge? *Earth and Planetary Science Letters*, *243*(3–4), 632–649. https://doi.org/10.1016/j.epsl.2006.01.022

Levin, V., Menke, W., & Park, J. (1999). Shear wave splitting in the Appalachians and the Urals: A case for multilayered anisotropy. *Journal of Geophysical Research*, *104*(B8), 17975–17993. https://doi.org/10.1029/1999jb900168

Li, J., Zheng, Y., Thomsen, L., Lapen, T. J., & Fang, X. (2018). Deep earthquakes in Subducting slabs hosted in highly anisotropic rock fabric. *Nature Geoscience*, *11*(9), 696–700. https://doi.org/10.1038/s41561-018-0188-3

Long, M. D., Hager, B. H., de Hoop, M. V., & van der Hilst, R. D. (2007). Two-dimensional modelling of subduction zone anisotropy with application to southwestern Japan. *Geophysical Journal International*, *170*(2), 839–856. https://doi.org/10.1111/j.1365-246x.2007.03464.x

Long, M. D., & van der Hilst, R. D. (2005). Upper mantle anisotropy beneath Japan from shear wave splitting. *Physics of the Earth and Planetary Interiors*, *151*(3–4), 206–222. https://doi.org/10.1016/j.pepi.2005.03.003

Long, M. D., & van der Hilst, R. D. (2006). Shear wave splitting from local events beneath the Ryukyu Arc: Trench-parallel anisotropy in the mantle wedge. *Physics of the Earth and Planetary Interiors*, *155*(3–4), 300–312. https://doi.org/10.1016/j.pepi.2006.01.003

Lynner, C., & Long, M. D. (2015). Heterogeneous seismic anisotropy in the transition zone and uppermost lower mantle: Evidence from south America, Izu-Bonin and Japan. *Geophysical Journal International*, *201*(3), 1545–1552. https://doi.org/10.1093/gji/ggv099

Mainprice, D., & Ildefonse, B. (2009). Seismic anisotropy of subduction zone minerals–contribution of hydrous phases. *Frontiers in Earth Sciences*, 63–84. https://doi.org/10.1007/978-3-540-87974-9_4

Mainprice, D., Le Page, Y., Rodgers, J., & Jouanna, P. (2007). Predicted elastic properties of the hydrous d phase at mantle pressures: Implications for the anisotropy of subducted slabs near 670-km discontinuity and in the lower mantle. *Earth and Planetary Science Letters*, *259*(3–4), 283–296. https://doi.org/10.1016/j.epsl.2007.04.053

Mallick, S., & Frazer, L. N. (1991). Reflection/transmission coefficients and azimuthal anisotropy in marine seismic studies. *Geophysical Journal International*, *105*(1), 241–252. https://doi.org/10.1111/j.1365-246x.1991.tb03459.x

Maupin, V., & Park, J. (2007). Theory and observations—Wave propagation in anisotropic media, In *Treatise on geophysics*. Series, Elsevier.

Nakajima, J., & Hasegawa, A. (2004). Shear-wave polarization anisotropy and subduction-induced flow in the mantle wedge of northeastern Japan. *Earth and Planetary Science Letters*, *225*(3–4), 365–377. https://doi.org/10.1016/j.epsl.2004.06.011

National Research Institute for Earth Science and Disaster Resilience. (2019). NIED Hi-net [Dataset]. *National Research Institute for Earth Science and Disaster Resilience*. https://doi.org/10.17598/NIED.0003

Nowacki, A., Kendall, J. M., Wookey, J., & Pemberton, A. (2015). Mid-mantle anisotropy in subduction zones and deep water transport. *Geochemistry, Geophysics, Geosystems*, *16*(3), 764–784. https://doi.org/10.1002/2014gc005667

Ozalaybey, S., & Savage, M. K. (1994). Double-layer anisotropy resolved from s phases. *Geophysical Journal International*, *117*(3), 653–664. https://doi.org/10.1111/j.1365-246x.1994.tb02460.x

Romanowicz, B., & Yuan, H. (2012). On the interpretation of SKS splitting measurements in the presence of several layers of anisotropy. *Geophysical Journal International*, *188*(3), 1129–1140. https://doi.org/10.1111/j.1365-246x.2011.05301.x

Saiga, A., Hiramatsu, Y., Ooida, T., & Yamaoka, K. (2003). Spatial variation in the crustal anisotropy and its temporal variation associated with a moderate-sized earthquake in the Tokai region, central Japan. *Geophysical Journal International*, *154*(3), 695–705. https://doi.org/10.1046/j.1365-246x.2003.01998.x

Salah, M. K., Seno, T., & Iidaka, T. (2009). Seismic anisotropy in the wedge above the Philippine sea slab beneath Kanto and southwest Japan derived from shear wave splitting. *Journal of Asian Earth Sciences*, *34*(1), 61–75. https://doi.org/10.1016/j.jseaes.2008.04.004

Saltzer, R. L., Gaherty, J. B., & Jordan, T. H. (2000). How are vertical shear wave splitting measurements affected by variations in the orientation of azimuthal anisotropy with depth? *Geophysical Journal International*, *141*(2), 374–390. https://doi.org/10.1046/j.1365-246x.2000.00088.x

Savage, M. K. (1999). Seismic anisotropy and mantle deformation: What have we learned from shear wave splitting? *Review of Geophysics*, *37*(1), 65–106. https://doi.org/10.1029/98rg02075

Shirey, S. B., Wagner, L. S., Walter, M. J., Pearson, D. G., & van Keken, P. E. (2021). Slab transport of fluids to deep focus earthquake depths—Thermal modeling constraints and evidence from diamonds. *AGU Advances*, *2*(2), e2020AV000304. https://doi.org/10.1029/2020av000304

Silver, P. G., & Chan, W. W. (1991). Shear-wave splitting and subcontinental mantle deformation. *Journal of Geophysical Research*, *96*(B10), 16429–16454. https://doi.org/10.1029/91jb00899

Silver, P. G., & Savage, M. K. (1994). The interpretation of shear-wave splitting parameters in the presence of 2 anisotropic layers. *Geophysical Journal International*, *119*(3), 949–963. https://doi.org/10.1111/j.1365-246x.1994.tb04027.x

Song, T. R. A., & Kawakatsu, H. (2012). Subduction of oceanic asthenosphere: Evidence from sub-slab seismic anisotropy. *Geophysical Research Letters*, *39*(17). https://doi.org/10.1029/2012gl052639

Song, T. R. A., & Kim, Y. (2012). Anisotropic uppermost mantle in young subducted slab underplating central Mexico. *Nature Geoscience*, *5*(1), 55–59. https://doi.org/10.1038/ngeo1342

Thomsen, L. (1986). Weak elastic anisotropy. *Geophysics*, *51*(10), 1954–1966. https://doi.org/10.1190/1.1442051

Thomsen, L. (1995). Elastic anisotropy due to aligned cracks in porous rock. *Geophysical Prospecting*, *43*(6), 805–829. https://doi.org/10.1111/j.1365-2478.1995.tb00282.x

Vavrycuk, V. (2004). Inversion for anisotropy from non-double-couple components of moment tensors. *Journal of Geophysical Research*, *109*(B7), B07306. https://doi.org/10.1029/2003jb002926

Vavrycuk, V. (2006). Spatially dependent seismic anisotropy in the Tonga subduction zone: A possible contributor to the complexity of deep earthquakes. *Physics of the Earth and Planetary Interiors*, *155*(1–2), 63–72. https://doi.org/10.1016/j.pepi.2005.10.005

Walsh, E., Arnold, R., & Savage, M. K. (2013). Silver and Chan revisited. *Journal of Geophysical Research: Solid Earth*, *118*(10), 5500–5515. https://doi.org/10.1002/jgrb.50386

Wang, J., Zhao, D. P., & Yao, Z. X. (2017). Seismic anisotropy evidence for dehydration embrittlement triggering intermediate-depth earthquakes. *Scientific Reports*, *7*(1), 2613. https://doi.org/10.1038/s41598-017-02563-w

Wirth, E., & Long, M. D. (2010). Frequency-dependent shear wave splitting beneath the Japan and Izu-Bonin subduction zones. *Physics of the Earth and Planetary Interiors*, *181*(3–4), 141–154. https://doi.org/10.1016/j.pepi.2010.05.006

Wüstefeld, A., Bokelmann, G., Zaroli, C., & Barruol, G. (2008). Splitlab: A shear-wave splitting environment in Matlab [Software]. *Computers & Geosciences*, *34*(5), 515–528. https://doi.org/10.1016/j.cageo.2007.08.002

Yu, C., Zheng, Y., & Shang, X. (2017). Crazyseismic: A Matlab Gui-based software package for passive seismic data preprocessing. *Seismological Research Letters*, *88*(2A), 410–415. https://doi.org/10.1785/0220160207

References From the Supporting Information

Kennett, B. L. N., & Engdahl, E. R. (1991). Traveltimes for global earthquake location and phase identification. *Geophysical Journal International*, *105*(2), 429–465. https://doi.org/10.1111/j.1365-246x.1991.tb06724.x